Preprints of the 21st IFAC World Congress (Virtual)
Berlin, Germany, July 12-17, 2020

Robotised Wire Arc Additive Manufacturing Using Set-based Control: Experimental Results

Linn Danielsen Evjemo *, **Signe Moe** *,**, **Jan Tommy Gravdahl** *

* *Department of Engineering Cybernetics, NTNU, Trondheim, Norway (e-mail: linn.d.evjemo@ntnu.no, signe.moe@ntnu.no, jan.tommy.gravdahl@ntnu.no)*
** *Department of Mathematics and Cybernetics, SINTEF Digital, Oslo, Norway*

Abstract: Additive manufacturing (AM) is a term that covers a variety of techniques for building custom-made, three dimensional structures. Such methods have moved from initially being used for creating simplified models to enable visualising of a product in a developing process, to creating structures that are suitable as end-products (Gibson et al., 2010). This has made prototyping and the production of custom made parts more accessible to small companies and developers, and AM technologies are still gaining momentum. However, traditional methods for AM are limited to building structures that are smaller than the AM apparatus itself, and bound to building structures layer by layer. The motivation for combining AM with a robot manipulator is to increase the workspace of the build, making it possible to build much larger structures, and to deposit material in any direction. The focus of this research is large-scale AM in metal, so the work presented in this paper focuses on a set-based control method for wire-arc additive manufacturing (WAAM) of a cylindrical, thin-walled structure. The set-based control method used to control the robot manipulator allows for some freedom in the orientation of the tool, so that the material is not necessarily deposited strictly vertically. Evaluating how this impacts the structure helps map how feasible this solution is for building more complex structures in future work.

Keywords: Additive Manufacturing, manufacturing systems, robot programming, set-based control. wire arc additive manufacturing

1. INTRODUCTION

Additive manufacturing (AM) is more commonly spoken of as 3D-printing, rapid prototyping (RP), or free-form fabrication. Most well-established methods for AM have strict limitations on size and geometry of the structures that is produced. Motivated by an aim to circumvent the main limitations that traditional AM methods face today, our research combine wire arc additive manufacturing (WAAM) with a 6 degrees-of-freedom (DOF) robot manipulator, and a set-based control method that allows for some freedom in the orientation of the welding gun. This freedom means that throughout the build, material is deposited in a mostly non-vertical manner, which differ strongly from traditional methods. Combining metal AM with freedom in orientation of the material deposition, and a non-layer-by-layer approach to the building process itself, makes this a novel idea.

1.1 Robotised WAAM

For traditional AM methods, the building process is in most cases done in-box, enclosed in an AM machine that must be larger than the structure it is building. It is only practical to expand the size of such an apparatus up to a certain point, which greatly limits the size of any structure that can be produced. Furthermore, traditional methods for AM methods primarily use a layer-by-layer approach, either building the structure strictly bottom-up or top-down. Since each layer has to be vertically attached to either the previous layer or some other means of support, the production of structures with overhangs depend upon additional support structures being built, which must again be removed post-build. A 6 DOF robot manipulator can move a tool attached to its end effector, e.g. a welding gun, to any point in its workspace with an arbitrary orientation, making it possible to deposit fast solidifying material in any direction. Moving away from the layer-wise approach could thereby remove the need for support structures, saving both time and material.

A focus of this research is to build metal structures using WAAM. The modified metal inert gas welding method cold metal transfer (CMT) is well suited for WAAM because is has a more stable arc which reduces metal splattering, and has a reduced heat-input which reduces residual stresses and distortions by refining the deposited microstructure (Cong et al., 2016). There is therefore an extra

Fig. 1. **Proof-of-concept:** Structure built with helix-path, but with a strictly vertical orientation of the tool (Evjemo et al., 2017).

focus on CMT in our research.

Building large components can be quite time consuming, with or without a strictly layer-wise approach: The height of each deposited welding bead affects the roughness of the finished surface, as well as the accuracy of the build compared to the model. If the surface is to be post-processed, and the level of detail in the build is therefore less important, one can increase how much material is deposited at a time, thereby making it possible to build quicker and bigger. It is still necessary to make such a build as effective as possible, so an objective for our research is to build continuously, both to save time and to make the structure less vulnerable to deformations due to flame-out and arc initiation when pausing the welding process (Evjemo et al., 2019).

1.2 Orientation of welding gun

The structures manufactured in the experiments presented here are built in aluminium, which has very low heat-emission to air and dissipates heat almost solely through conduction (Geng et al., 2017). Earlier tests have shown that accumulation of heat in structures built in materials as soft as aluminium will more easily lead to deformations compared to structures build in harder metals such as nickel (Evjemo et al., 2019). All the experiments presented in (Evjemo et al., 2017) and (Evjemo et al., 2019) were conducted with a fixed, vertical orientation of the welding gun on a horizontal surface. If the flexibility of the robot manipulator can be used in such a way that it is no longer necessary to keep a strictly vertical orientation of the welding gun, it might be possible to gain more flexibility in the building process. This could allow for a longer cool-down period in parts of the structure that require it, without the need to pause the build.

This paper presents how a thoroughly tested method for set-based control was used to program the robot's path, including some freedom in the orientation of the tool, thereby increasing the flexibility of the build. Others have worked on making AM more flexible by building on a tilting surface, with a fixed point of material deposition. This has been performed both in plastic using a 6 DOF robot manipulator (Dai et al., 2018), and in metal (Panchagnula and Simhambhatla, 2018). However, the focus of our research is to see how a robot manipulator can deposit material on a fixed surface with a not strictly vertical orientation of the tool. Joris Laarbman Lab have produced very promising results on similar work, using both a fast-curing polymer (Laarman et al., 2014) and stainless steel (Jorislaarman.com, 2015-2019), but none of their algorithms or methods have been made public.

The aim was to build a cup structure similar to the one built in viscous glue in the proof-of-concept experiments from 2017 (Evjemo et al., 2017), seen in Figure 1. As a consequence of using a soft building material, the original glue cup was built very small, with a radius of 2 cm. These new structures in aluminium are built much larger: The radius was set to 8 cm, in the hopes that heat would dissipate quickly enough to enable a continuous build. The method for set-based control, presented in Section 2, allowed for additional freedom in the orientation of the welding gun. The aim of these experiments was to show how robotised WAAM can better take advantage of the flexibility of a 6 DOF robot manipulator. An objective was also to investigate how additional freedom in the orientation of the welding gun will affected the build, and if this is a promising method going forward.

The rest of this paper is organized as follows: In Section 2, the theory behind the set-based control method used in these experiments is explained. The results and data from the experiments are presented in Section 3. The results are then evaluated and discussed in Section 4. Finally, some concluding remarks are discussed in Section 5.

2. THEORY: SET-BASED CONTROL

The aim of the experiment was to construct a large, cylindrical shape built with the same path as the cup from the initial experiments presented in (Evjemo et al., 2017). This path already deviates from traditional AM methods in the sense that the structure is not built layer-wise, but with a continuous vertical motion creating a helix, see Figure 2. As with the glue cup shown in Figure 1, a bottom layer was included by depositing material in an outwards spiral.

To allow some freedom in the orientation of the welding gun, a set-based framework was used to control the joints of the robot manipulator. This framework is particularly suited for robotic systems with a large number of DOFs and several tasks to solve. Furthermore, it allows for set-based tasks defined by a valid interval (such as collision avoidance) in addition to equality tasks defined by an exact desired value (e.g. position control). For an extensive description of the framework and its properties, the interested reader is referred to (Moe et al., 2016; Moe et al., 2018).

Typically, the desired behaviour of a robot is described in task space, whereas the robot is actually controlled in the joint space. Set-based control is a kinematic control

framework which calculates reference states based on the desired behaviour and the current state of the system.

A general robotic system has n DOFs and its configuration is given by the joint values $\boldsymbol{q} = [q_1, q_2, \ldots, q_n]^T$. The system tasks and task velocities are described through forward kinematics and the Jacobian matrix. For instance, a task $\boldsymbol{\sigma}(t) \in R^m$ can be expressed as

$$\boldsymbol{\sigma}(t) = \boldsymbol{f}(\boldsymbol{q}(t)), \tag{1}$$

where $\boldsymbol{f}(\boldsymbol{q}(t))$ is the forward kinematics, which can be derived for instance through the Denavit-Hartenberg convention (Spong and Hutchinson, 2005). The time-derivative of the task is given as

$$\dot{\boldsymbol{\sigma}}(t) = \frac{\partial \boldsymbol{f}(\boldsymbol{q}(t))}{\partial \boldsymbol{q}} \dot{\boldsymbol{q}}(t) = \boldsymbol{J}(\boldsymbol{q}(t))\dot{\boldsymbol{q}}(t), \tag{2}$$

where $\boldsymbol{J}(\boldsymbol{q}(t)) \in R^{m \times n}$ is the Jacobian matrix and $\dot{\boldsymbol{q}}(t) \in R^n$ is the system velocity. For compactness, the argument $\boldsymbol{q}$ of tasks and Jacobians are omitted from the equations for the remainder of this section.

Consider a single m-dimensional equality task with a defined desired trajectory $\boldsymbol{\sigma}_{\text{des}}(t) \in R^m$. The corresponding joint references $\boldsymbol{q}_{\text{des}}(t) \in R^n$ may be computed by integrating

$$\dot{\boldsymbol{q}}_{\text{des}} = \boldsymbol{J}^{\dagger}\Big(\dot{\boldsymbol{\sigma}}_{\text{des}} + \boldsymbol{\Lambda}\tilde{\boldsymbol{\sigma}}\Big), \tag{3}$$

where $\boldsymbol{J}^{\dagger}$ is the pseudoinverse of $\boldsymbol{J}$, $\tilde{\boldsymbol{\sigma}} = \boldsymbol{\sigma}_{\text{des}} - \boldsymbol{\sigma}$ is the task error and $\boldsymbol{\Lambda} \in R^{m \times m}$ is a positive-definite matrix of gains.

In these experiments, we consider two tasks to achieve welding: Position control $\boldsymbol{\sigma}_{\text{pos}}(\boldsymbol{q}) \in R^3$ of the end effector to follow the defined welding trajectory and field of view (FOV) $\sigma_{\text{FOV}} \in R$. The latter is defined as the angle between the outgoing unit vector of the end effector, i.e. the direction it is pointing when depositing material, and a vertical vector. In traditional welding and in previous experiments conducted by the authors, σ_{FOV} is defined as en equality task with $\sigma_{\text{FOV, des}} = 0°$, corresponding to maintaining a constant orientation of the end effector normally to the welding surface. However, to allow some freedom in the orientation when depositing materials, σ_{FOV} is considered a set-based task in these experiments. This approach has shown promising results in similar applications such as spray painting (Moe et al., 2018).

For a set-based task $\sigma \in R$, the desired behaviour is not defined by an explicit σ_{des}, but $\sigma \in [\sigma_{\min}, \sigma_{\max}] \ \forall \ t \geq t_0$. The set-based control framework handles a set-based task by ignoring them and letting the motion be controlled only by the equality tasks until such a time this would result in the set-based task leaving its valid set. This is considered mode 1 of the system. However, should mode 1 result in the set-based task leaving its valid set, it is actively inserted into the kinematic controller with the goal of keeping it on the limit of the valid set. This is mode 2 of the system, which is active until such a time that controlling only the equality tasks will naturally bring the set-based task into the valid set. Since the set-based task σ_{FOV} in these experiments is defined as the angle between the FOV of the end effector and a vertical vector, the valid set is defined as $C_{\text{FOV}} = \left[0°, \sigma^{\circ}_{\text{FOV, max}}\right]$. In mode 1, σ_{FOV} is ignored and the desired motion of the robot is determined based on position control and the desired welding trajectory. In mode 2, σ_{FOV} is actively controlled to its maximum limit to prevent the task from being violated. Thus, the two modes are defined as

$$\begin{aligned} \dot{\boldsymbol{q}}_{1,\text{des}} &= \boldsymbol{J}^{\dagger}_{\text{pos}}\left(\dot{\boldsymbol{\sigma}}_{\text{pos, des}} + \boldsymbol{\Lambda}_1\tilde{\boldsymbol{\sigma}}_{\text{pos}}\right), \\ \dot{\boldsymbol{q}}_{2,\text{des}} &= \begin{bmatrix} \boldsymbol{J}_{\text{pos}} \\ \boldsymbol{J}_{\text{FOV}} \end{bmatrix}^{\dagger} \left(\begin{bmatrix} \dot{\boldsymbol{\sigma}}_{\text{pos, des}} \\ 0 \end{bmatrix} + \boldsymbol{\Lambda}_2 \begin{bmatrix} \boldsymbol{\sigma}_{\text{pos, des}} - \boldsymbol{\sigma}_{\text{pos}} \\ \sigma_{\text{FOV, max}} - \sigma_{\text{FOV}} \end{bmatrix} \right). \end{aligned} \tag{4}$$

The switching between modes is determined in Algorithm 2 using the tangent cone (Algorithm 1). In general, the tangent cone algorithm returns True 1) if the task is in its valid interval or 2) if it is outside the valid interval but moving towards it. Algorithm 2 evaluates whether or not this is the case for σ_{FOV} given Mode 1, i.e. if controlling the joints based only on the position task ($\dot{\boldsymbol{q}}_{1,\text{des}}$) will lead σ_{FOV} out of its valid interval. For further details, see (Moe et al., 2016; Moe et al., 2018).

Algorithm 1 The boolean function in_T_C.

Input: σ, $\dot{\sigma}$, $\sigma_{\min}$, $\sigma_{\max}$
if $\sigma_{\min} < \sigma < \sigma_{\max}$ **then**
  return True
else if $\sigma \leq \sigma_{\min}$ *and* $\dot{\sigma} \geq 0$ **OR** $\sigma \geq \sigma_{\max}$ *and* $\dot{\sigma} \leq 0$ **then**
  return True
else
  return False
end

Algorithm 2 Activation of modes.

a = in_T_C(σ_{FOV},$\boldsymbol{J}_{\text{FOV}}\dot{\boldsymbol{q}}_{1,\text{des}}$,0,$\sigma_{\text{FOV,max}}$)
if *a is True* **then**
  $\dot{\boldsymbol{q}}_{\text{des}} = \dot{\boldsymbol{q}}_{1,\text{des}}$
else
  $\dot{\boldsymbol{q}}_{\text{des}} = \dot{\boldsymbol{q}}_{2,\text{des}}$
end

The trajectory consists of an outwards spiralling bottom which moves over to an upwards helix when the desired radius for the bottom is reached, shown in Figure 2. As in (Evjemo et al., 2017), each point on the spiral trajectory is expressed in cylindrical coordinates θ, r, and z. We define h as the height difference between each bead or layer in the wall, and r_1 as the horizontal distance between each bead in the bottom. H is the desired final height of the structure, and R is the desired radius. All of these variables are given in meters. r and z are defined as functions of θ:

$$r(\theta) = \begin{cases} \frac{r_1}{2\pi}\theta & \theta \leq \frac{R}{r_1}2\pi \\ R & \theta > \frac{R}{r_1}2\pi \end{cases} \tag{5}$$

$$z(\theta) = \begin{cases} 0 & \theta \leq \frac{R}{r_1}2\pi \\ \frac{h}{2\pi}(\theta - \frac{R}{r_1}2\pi) & \theta > \frac{R}{r_1}2\pi \end{cases} \tag{6}$$

Thus, the time-derivatives of r and z are given by:

$$\dot{r}(\theta) = \begin{cases} \frac{r_1}{2\pi}\dot{\theta} & \theta \leq \frac{R}{r_1}2\pi \\ 0 & \theta > \frac{R}{r_1}2\pi \end{cases} \tag{7}$$

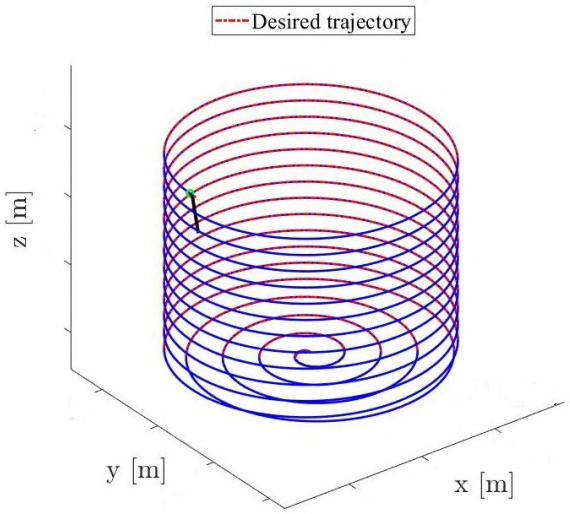

Fig. 2. **Helix path:** The dimensions in this plot is exaggerated in order to more easily illustrate the path.

$$\dot{z}(\theta) = \begin{cases} 0 & \theta \leq \frac{R}{r_1} 2\pi \\ \frac{h}{2\pi}\dot{\theta} & \theta > \frac{R}{r_1} 2\pi \end{cases} \tag{8}$$

where $\dot{\theta}$ is defined as:

$$\dot{\theta} = \begin{cases} \frac{2\pi U}{r_1\sqrt{\theta^2+1}} & \theta \leq \frac{R}{r_1} 2\pi \\ \frac{U}{\sqrt{R^2+\frac{h}{2\pi}^2}} & \theta > \frac{R}{r_1} 2\pi \end{cases} \tag{9}$$

$\dot{\theta}$ is chosen such that the end effector velocity along the trajectory is constant and equal to the desired velocity U, which is necessary for even deposition of metal.

To express the desired end effector position in Cartesian coordinates, we rewrite the trajectory given in cylindrical coordinates (5)-(6) through the following transformation:

$$\begin{aligned} x_{des} &= r(\theta)\cos\theta \\ y_{des} &= r(\theta)\sin\theta \\ z_{des} &= z(\theta) \end{aligned} \tag{10}$$

Thus, the time derivatives are given as:

$$\begin{aligned} \dot{x}_{des} &= \dot{r}(\theta)\cos\theta - r(\theta)\sin\theta\dot{\theta}(\theta) \\ \dot{y}_{des} &= \dot{r}(\theta)\sin\theta + r(\theta)\cos\theta\dot{\theta}(\theta) \\ \dot{z}_{des} &= \dot{z}(\theta) \end{aligned} \tag{11}$$

where $\dot{r}$, $\dot{z}$, and $\dot{\theta}$ are defined in (7)-(9). Thus, the commanded joint velocity is defined in (3) with $\boldsymbol{\sigma}_{\text{pos}} = [x_{des}, y_{des}, z_{des}]^T$ and $\dot{\boldsymbol{\sigma}}_{\text{pos}} = [\dot{x}_{des}, \dot{y}_{des}, \dot{z}_{des}]^T$.

In the experiments presented in this paper, the following numeric values are used:

- U is 0.10 m/s, based on tests in (Evjemo et al., 2019).
- R is 0.08 m
- r_1 is between 4.0 mm and 4.5 mm, see Tables 1-4
- h is between 12 mm and 14 mm, see Tables 1-4

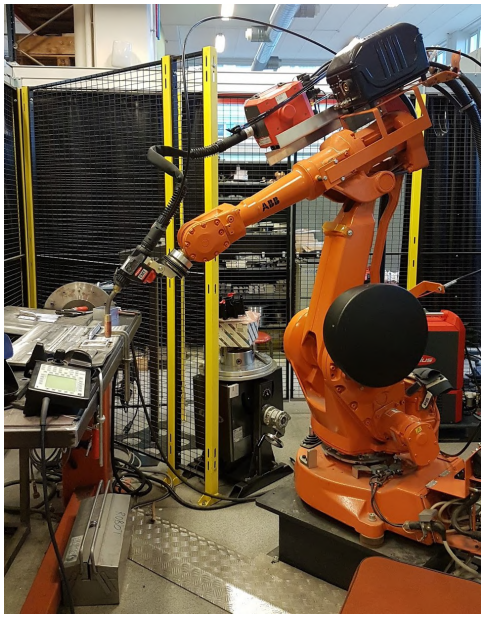

Fig. 3. **Experimental set-up:** 6 DOF ABB IRB2400/10 robot manipulator with welding equipment from Fronius.

- The freedom in orientation $\sigma^{\circ}_{\text{FOV, max}}$ is between 0 and 10

3. EXPERIMENTAL RESULTS

These experiments were performed in collaboration with SINTEF Industry using a 6 DOF IRB 2400/10 robot manipulator from ABB Robotics (Abb.com, 2016-2018) with an attached metal inert gas (MIG) welding gun with CMT technology developed by Fronius, see Figure 3. The metal cylinder structure shown in Figure 4 was built in order to have some grounds of comparison between a build done with and without deviations in the orientation of the welding gun. It was built using the RAPID programming language from ABB, just as the structures referenced in (Evjemo et al., 2019). The vertical position of the welding gun was increased continuously throughout the build, creating a helix path, thereby avoiding traditional layers.

The base plate for all the builds presented here was made of the aluminium alloy 6082-T6, and was approx. 15 mm thick. The welding wire was of the aluminium alloy AlMg4.5Mn. For the purpose of documenting the experiments presented in this paper, the welding parameters are given for each *approximate* layer in Table 1 to 4. This should be interpreted as that the current etc. was adjusted after approx. this number of full rotations in the upwards helix path from Figure 2.

3.1 Test 1: Pulsed MIG, fixed orientation of welding gun

Because of the before-mentioned benefits of using CMT, such as reduced metal splattering and less residual stresses, the aim was to use this method for as much of the building process as possible. On the other hand, work presented in (Evjemo et al., 2017) and (Evjemo et al., 2019) show

Fig. 4. **Vertical welding gun:** Cylindrical structure built with fixed, vertical orientation of the welding gun, with continuous height increase like that shown in Figure 2.

that there are significant benefits to building as continuously as possible, ideally avoiding breaks in the welding process altogether. The metal plate used as base in these experiments was thicker than the base used in earlier tests, which meant that the distortions of the base plate due to the heating and cooling of the metal should be less prominent. However, this also meant that the first part of the build, the spiralling bottom, had to be welded with a higher heat-input than the rest of the structure in order for the weld to adhere properly to the base (Evjemo et al., 2019). The heat-input available when using CMT technology was not sufficient, so the bottom part of the cup instead had to be welded using pulsed MIG welding, which allows for a scientifically higher heat-input than CMT.

In our experimental set-up, it was not possible to change welding methods without pausing the welding process. This was not ideal, and made it necessary to make the choice between an uninterrupted build and the very controlled welding process that CMT could provide. Focusing on doing a continuous build, test 1 was done without interruption using only pulsed MIG welding. Based on experience from earlier experiments presented in (Evjemo et al., 2019), the layer height was set to 1.2 mm, and the radius of the cylinder was set to 60 mm. As the thickness of the thin-walled structure shown in Figure 4 was approx. 4 mm, the horizontal distance between layers in the spiralling bottom layer was also set to 4 mm.

Test 1 stopped after 4-5 layers after with the error message "Wire buffer full" on the welding equipment. This was due to over heating of the soft aluminium wire when using Pulsed MIG over time, a problem that had not been encountered when working with harder metals with a higher melting point such as the nickel alloy Inconel625 (Evjemo et al., 2019). The build from test 1 is shown to the top left of Figure 5.

Table 1. Welding param. for test 1: Pulsed MIG welding and fixed orientation of welding gun.

Test 1: Pulsed MIG				
Layer number	**Current** (A)	**Wire feed sp.** (m/min)	**Voltage** (V)	**Bead w.** (mm)
bottom	180	10.5	22.0	4.0
bottom	165	9.5	21.5	4.0
$\approx$ **1**	120	7.0	18.7	1.2
$\approx$ **2**	100	5.9	17.9	1.2
$\approx$ **3**	85	5.0	17.2	1.2
$\approx$ **4-5**	71	4.3	16.4	1.2

Fig. 5. **Set-based control:** The structures built in the first three tests, and close-up of the bottom.

3.2 Test 2: Pulsed MIG + CMT, fixed orientation of welding gun

As test 1 was interrupted, the second test was also done with a fixed orientation of the welding gun. The estimated bead width in the spiralling bottom was increased from 4.0 mm to 4.5 mm, as the overlap between the beads in the spiral was slightly too large. In order to avoid the wire feed issue from test 1, which seemed to be caused by overheating, the second test was performed using CMT welding. The thick metal base still made it necessary to weld the bottom with a higher heat-input, and the welding parameters from test 1 had seemingly worked well for this part of the build. The combination of pulsed MIG and CMT welding was introduced: When the robot moved from the part of the path that was the spiralling bottom layer on to the helix walls, the process was manually interrupted and paused. The settings for welding method was changed manually from pulsed MIG to CMT, before the welding process continued.

The welding parameters for this test are listed in Table 2. Test 2 was interrupted after completing the bottom and building approx. 14 rotations of wall because the tip of the welding gun ended up too close to the surface.

Table 2. Welding param. for test 2: Pulsed MIG + CMT welding and fixed orientation of welding gun.

Test 2: Pulsed MIG + CMT				
Pulsed MIG on bottom layer				
Layer number	**Current** (A)	**Wire feed sp.** (m/min)	**Voltage** (V)	**Bead w.** (mm)
bottom	180	10.5	22.0	4.5
bottom	160	9.2	21.3	4.5
Beginning of walls, changed to CMT				
≈ **1**	135	9.0	15.0	1.2
≈ **2**	115	8.2	14.3	1.2
≈ **3-4**	80	5.2	11.8	1.2
≈ **5-14**	75	4.8	11.7	1.2

The estimated height of each layer of deposited material was set to 1.2 mm based on previous builds, but the decreasing distance between the structure and the welding gun indicated that this should be increased for the next tests. In addition, the metal base contracted more than anticipated, so the welding gun was placed slightly higher above the base at the beginning of the welding process to counteract this.

3.3 Test 3: Pulsed MIG + CMT, set-based control of welding gun orientation

Because tests 1 and 2 had shown how much the metal base would bend and contract when heating up, the welding gun was placed approx. 16 mm above the base, as opposed to approx 11 mm for tests 1 and 2. In addition, the estimated height of each layer of deposited material was increased from 1.2 mm to 1.4 mm. The estimated width of the welding bead was kept to 4.5 mm, as the bottom layer from test 2 was smoother than that from test 1. Freedom for the orientation of the welding gun was included, which allowed for up to 10° deviation in angle relative to a vertical orientation.

The large heat-input from the pulsed MIG welding used when building the bottom lead the whole structure to heat up in a way that seemed to make the ensuing deposition of material uneven. As can be seen to the top right of Figure 5, the walls became quite uneven compared to earlier experiments (Evjemo et al., 2019) or the reference structure shown in Figure 4. Therefore, some active cooling was added to the process: When the welding was paused in order to change from pulsed MIG to CMT, cool air was blown onto the structure for approx. 30 seconds in order for it to cool down.

This build was only programmed to be 4 cm tall, and completed without complications. The result can be seen to the bottom left of Figure 5.

3.4 Test 4: Pulsed MIG + CMT, set-based control of welding gun orientation

Test 3 was overall successful, but the complete structure was only 4 cm tall. The aim of test 4 was therefore to keep most of the parameters from test 3, including the manual interruption in order to change welding methods, and build a taller structure. The estimated bead width in the bottom layer was kept at 4.5 mm, and the estimated height of each layer of deposited material was kept at 1.4 mm. The freedom in orientation angle was set to 6°. The build completed without complications. The welding parameters are listed in Table 4, and the final structure is shown in Figure 6. The active cooling when swapping from pulsed MIG to CMT was also included for this build.

Table 3. Welding param. for test 3: Pulsed MIG + CMT welding and set-based control of orientation of welding gun.

Test 3: Pulsed MIG + CMT				
Pulsed MIG on bottom layer				
Layer number	**Current** (A)	**Wire feed sp.** (m/min)	**Voltage** (V)	**Bead w.** (mm)
bottom	180	10.5	22.0	4.5
bottom	168	9.7	21.6	4.5
Beginning of walls, changed to CMT. Some active cooling.				
≈ **1**	135	9.0	15.0	1.4
≈ **2**	116	8.9	14.3	1.4
≈ **3**	100	7.0	13.8	1.4
≈ **4-5**	85	5.5	11.9	1.4
≈ **6-7**	80	5.2	11.8	1.4
≈ **8-28**	75	4.8	11.7	1.4

Table 4. Welding param. for test 4: Pulsed MIG + CMT welding and set-based control of orientation of welding gun.

Test 4: Pulsed MIG + CMT				
Pulsed MIG on bottom layer				
Layer number	**Current** (A)	**Wire feed sp.** (m/min)	**Voltage** (V)	**Bead w.** (mm)
bottom	180	10.5	22.0	4.5 mm
bottom	168	9.7	21.6	4.5
Beginning of walls, changed to CMT. Some active cooling.				
≈ **1**	135	9.0	15.0	1.4
≈ **2**	116	8.9	14.3	1.4
≈ **3**	100	7.0	13.8	1.4
≈ **4-5**	85	5.5	11.9	1.4
≈ **6-105**	80	5.2	11.8	1.4

Fig. 6. **Set-based:** The tallest cylinder structure.

4. DISCUSSION

The spiral making out the bottom of the cup was very smooth, with few deformations, as shown to the bottom right in Figure 5. This was somewhat surprising, as earlier welding experiments had shown that the arc initiation could easily be a source for distortions in the structure (Evjemo et al., 2019). Building the same shape

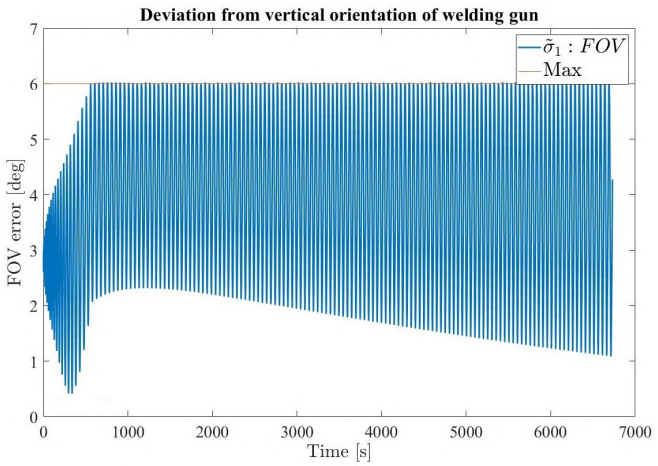

Fig. 7. **Orientation:** This is the $\sigma^{\circ}_{\text{FOV}}$ along the 4^{th} build. It ends up going back and forth from approx. 1° and 6°.

in a smaller version made out of viscous glue had also shown that material would easily heap up in the centre of the spiral, due to continuous material deposition in a very small area (Evjemo et al., 2017). The reason why this worked much better in these latest builds is likely that the high heat-input provided by the use of pulsed MIG welding meant that the metal was hot enough to properly melt together with the metal base, and subsequently the already deposited metal bead.

The method for set-based control is meant to simplify the movements of the robot by defining the position control of the end effector a set to stay within rather than a strict value to follow, as explained in Section 2. As can be seen in Figure 6, the tallest build ended up having a slight saddle form, even though the robot's path was meant to result in a cylinder with a flat top. This is likely due to the difference in orientation of the welding gun on the right side of the build compared to the left side. The build was done on a base that was not placed directly in front of the robot's base, but about 20 cm to the left. The result was therefore that the welding gun was more orthogonal to the surface on the side of the structure closest to the central axis of the robot, and had more of an angle on the side of the structure furthest away from the base. The deviation from a vertical orientation of the welding gun during the 4^{th} test is plotted in Figure 7: On one side of the structure, the limit of 6° is reached but not broken. On the other side, the deviation reaches a maximum of 2°, before slowly decreasing, almost coming back to 1° at the end of the build.

The difference in orientation of the welding gun was decided by the metal base's placement relative to the robot. The orientation of the welding gun determines how the material is deposited, and how the metal spreads out on the existing build, as gravity works on the liquid metal during deposition (Xiong et al., 2017). If the difference in the orientation of the welding gun could be more evenly distributed around some kind of centre point of the structure, so that the additional gravitational pull on the liquid metal would be evenly spread out over the circular path, it seems likely that the result would be more even. It should therefore be considered if the set-based control method can somehow be manipulated to prioritise a condition of moving around a centre point for the orientation over the freedom of the robot's movements.

The program used for controlling the robot in these experiments did not itself separate between building the bottom and the walls. The robot was given a list of joint angles generated by the set-based control system presented in Section 2, and moved between these configurations with a provided speed. Because the welding method had to be changed between the bottom and the walls in tests 2 to 4, the process had to be paused manually by the human operator when the bottom was built. It was somewhat challenging to evaluate in real-time when the bottom was completed by looking at the welding process while wearing a protective welding helmet. In one of the tests, the program was in fact paused too early, changing the welding method to CMT before the two final beads of the bottom layer was deposited. This did not change the resulting build dramatically, as the structure was already hot enough for the deposited metal to adhere properly to the base even when using CMT and a lower current.

During test 2 (Section 3.2), the build had to be interrupted due to an increasing distance between the welding gun and the surface. The height of each welding bead is determined by both the welding current, the temperature of the existing structure, and the gravitational pull when welding with a non-vertical orientation of the welding gun. This makes it difficult to accurately anticipate what the height difference h each bead in the walls should be, even with experience from previous builds. Actively adjusting this value during the build could help solve this, and keep the building process going. This was done in (Evjemo et al., 2019), but that solution meant that the welding process had to be paused shortly while the adjustments were made. Even though the manual changing of welding methods in the most recent experiments also required a short pause in the welding process during the build, continuity was an important objective. Adjusting h this way was therefore not considered a viable solution, and not used in the latest tests.

5. CONCLUDING REMARKS

The work presented in this paper has shown that continuous WAAM with some freedom in the orientation of the welding gun is possible, but that the deviation in orientation should to some extend be evenly distributed over the structure. If not, gravity can lead to unexpected deviations, such as the saddle form in the structure built in test 4 (Figure 6). If the set-based control method could be manipulated to distribute the deviation in orientation around a structural centre point, that might help solve this issue. However, this is not necessarily straight forward, as the main motivation of the set-based method is to prioritise the ease of the joint configurations.

The structures built in these experiments have taken advantage of the robot's manipulator's freedom in orientation as well as in position, unlike the work presented

in (Evjemo et al., 2017) and (Evjemo et al., 2019). Not relying on a strictly fixed orientation of the welding gun expands the available workspace for the build when performing WAAM by robot. If the build is done near the limits of the robot's workspace, introducing some freedom in orientation could help make a path feasible. Considering a lab or factory situation, a non-vertical orientation of the tool could make it possible to build around obstacles, either external ones or existing parts of the build. The next step of this research should be to build a more complex structure with overhang, which traditional AM methods cannot construct without adding additional support structures that must be removed in post-processing.

Manually pausing the build to change welding methods when necessary was challenging, because it was difficult to accurately determine when the bottom was finished just by observing the welding process thorough a welding mask. Even though pausing the program a bit early did not change the resulting build dramatically, the manual changing of welding methods was something that made it difficult to accurately re-produce an experiment. An important part of future work would be to remove the need for manually interrupting the welding process in order to change welding method. It might still be necessary to pause the welding process in order for the metal to cool down after the intense heat input provided by pulsed MIG welding, either naturally or through active cooling. If this could be included in the programming, it would still remove some of the inconsistencies that might arise when a human operator tries to manually pause the process at a given point, and thereby help create a build that is easier to re-produce.

Some way of monitoring the build should also be addressed in future work. This could either be external monitoring, such as cameras, or monitoring of the welding process itself by monitoring the currents and other welding parameters. A change in distance between the wire in the welding gun and the surface of the structure will impact the current, so monitoring this can help tell a lot about how smooth the structure is, if the distance between the welding gun and surface is increasing or decreasing, etc. Future work should also include designing and/or implementing control algorithms to help adjust the robot's path in order to correct for geometrical deviations based on the monitoring data. Implementing a way to actively adjust the height increase h between each bead in the walls should be included in this work, to help keep the build going even if the estimated h deviates from how the physical result.

ACKNOWLEDGEMENTS

The work reported in this paper was based on activities within centre for research based innovation SFI Manufacturing in Norway, and is partially funded by the Research Council of Norway under contract number 237900. Mr. Morten H. Danielsen is acknowledged for his experimental guidance related to arc welding.

REFERENCES

Abb.com (2016-2018). IRB 2400. URL `https://new.abb.com/products/robotics/industrial-robots/irb-2400`. Accessed 2018-10-22.

Cong, B., Ouyang, R., Qi, B., and Ding, J. (2016). Influence of cold metal transfer process and its heat input on weld bead geometry and porosity of aluminum-copper alloy welds. *Rare Metal Mat. Eng.*, 45(3), 606–611.

Dai, C., Wang, C.C., Wu, C., Lefebvre, S., Fang, G., and Liu, Y.J. (2018). Support-free volume printing by multi-axis motion. *ACM Transactions on Graphics (TOG)*, 37(4), 134.

Evjemo, L.D., Langelandsvik, G., and Gravdahl, J.T. (2019). Wire arc additive manufacturing by robot manipulator: Towards creating complex geometries. In *5th IFAC ICONS, Belfast*, 103–109. Elsevier.

Evjemo, L.D., Moe, S., Gravdahl, J.T., Roulet-Dubonnet, O., Gellein, L.T., and Brøtan, V. (2017). Additive manufacturing by robot manipulator: An overview of the state-of-the-art and proof-of-concept results. In *22nd IEEE ETFA, Cyprus*, 1–8.

Geng, H., Li, J., Xiong, J., and Lin, X. (2017). Optimisation of interpass temperature and heat input for wire and arc additive manufacturing 5A06 aluminium alloy. *Sci. Technol. Weld. Joi.*, 22(6), 472–483.

Gibson, I., Rosen, D.W., and Stucker, B. (2010). *Additive manufacturing technologies*, volume 238. Springer.

Jorislaarman.com (2015-2019). MX3D bridge. URL `https://www.jorislaarman.com/work/mx3d-bridge/`. Accessed 2019-11-11.

Laarman, J., Jokic, S., Novikov, P., Fraguada, L.E., and Markopoulou, A. (2014). Anti-gravity additive manufacturing. *Fabricate: Negotiating Design & Making*, 192–197.

Moe, S., Antonelli, G., Teel, A.R., Pettersen, K.Y., and Schrimpf, J. (2016). Set-Based Tasks within the Singularity-Robust Multiple Task-Priority Inverse Kinematics Framework: General Formulation, Stability Analysis, and Experimental Results. *Frontiers in Robotics and AI*, 3(April), 1–18. URL `http://journal.frontiersin.org/article/10.3389/frobt.2016.00016`.

Moe, S., Gravdahl, J.T., and Pettersen, K.Y. (2018). Set-based control for autonomous spray painting. *IEEE Transactions on Automation Science and Engineering*, 15(4), 1785–1796. doi:10.1109/TASE.2018.2801382.

Panchagnula, J.S. and Simhambhatla, S. (2018). Manufacture of complex thin-walled metallic objects using weld-deposition based additive manufacturing. *Robot. Com.-Int. Manuf.*, 49, 194–203.

Spong, M.W. and Hutchinson, S. (2005). *Robot Modeling and Control*. Wiley.

Xiong, J., Lei, Y., Chen, H., and Zhang, G. (2017). Fabrication of inclined thin-walled parts in multi-layer single-pass gmaw-based additive manufacturing with flat position deposition. *Journal of Materials Processing Technology*, 240, 397–403.